Continuous Error Correction in Quantum Dot Qubits

Stasiu Wolanski, Jesus College

2022 - 2023

Abstract

Woop!

Contents

0.1   Introduction

Chapter 1

Background

1.1 Quantum error correction

1.1.1 Quantum computing

1.1.2 Error correction

1.1.3 Continuous error correction

1.2 Quantum Dot Qubits

1.2.1 Semiconductor Heterostructures

The Hubbard Model

Chapter 2

Theory

2.1 Rapidly repeated error correction schemes

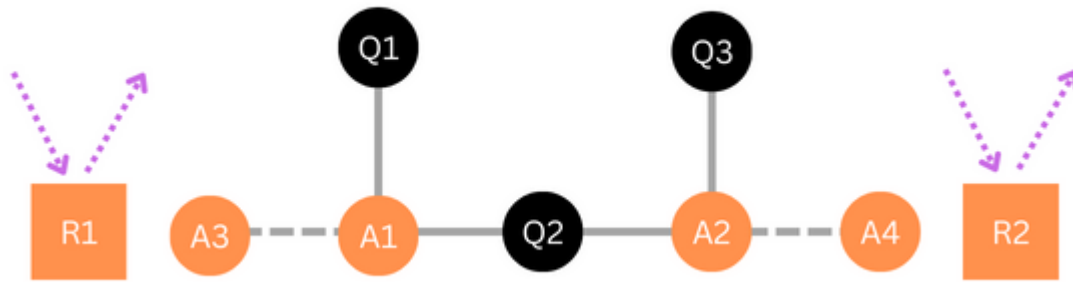## 2.2 Truly continuous error correction in quantum dot systems

Figure 2.1: Schematic of the layout of qubits for the continuous error correction scheme. Q1, Q2 and Q3 comprise a single logical qubit. A1 to A4 are ancilla qubits used to detect bit flip errors in the logical qubits. Q1 and Q2 are continuously weakly coupled to A1 through a tunnel barrier, and likewise Q2 and Q3 to A2. R1 and R2 are resonators, which are additional quantum dots held at a higher electron occupancy than the qubits. These are probed using RF signals, and their coupling to the charge on the ancillas then allows the singlet/triplet state of the ancillas, as in [2].

2.2.1 Scheme summary

In this section a proposal for truly continuous error correction is developed. I thank Chris Long, Dr Mertig, Giovanni Oakes and my supervisor Dr Arvidsson-Shukur for contributing variously to the development of the ideas presented here. Recent developments in the field of RF reflectometry measurements enable the measurement of the singlet/triplet state of two adjacent qubits coupled via a tunnel barrier, by monitoring the rf reflection characteristics of a neighbouring electron reservoir [2]. The codespace qubits are to be coupled pairwise to two ancilliary qubits whose function is to perform parity measurements, in such a way that any deviation from the codespace will result in a change of state of one or both of the ancilla qubits, depending on the error syndrome. The rate at which the error propogates to the ancilla qubit(s) is in the tens of nanoseconds, a faster timescale than either gate times (hundreds of nanoseconds) or readout (the state of the art [2] achives 6µs).

This scheme is potentially more efficient than a repeated error correction scheme like those analysed in section 2.1. One reason for this is that the 'dead time' after an error has occurred during which the system is vulnerable to a second error is limited by the time for the ancilla to be reset, which is also on the order of microseconds (e.g. see [1]). A second, more significant advantage is that the scheme does not require any quantum gates to be performed for the purposes of error sydrome detection, as such detection happens continuously and simultaneously with circuit

gates. This reduces circuit complexity, and avoids the error accumulation associated with performing the syndrome measurements.

TODO flesh this out.

The proposed qubit layout is given in figure 2.1. In the scheme, the logical qubit is encoded in the *odd parity subspace* of three qubits Q1, Q2, and Q3. There are two pairs of ancilla qubits: A1, A3, and A2, A4. Each of these is initially prepared in the T_0 triplet state. As shown in the figure, each pair of qubits Q1 and Q2, Q2 and Q3, is weakly coupled to one ancilla qubit through a voltage-controlled tunnel barrier. If the couplings are sufficiently well-tuned, the ancilla qubits will remain as triplets and no tunneling will occurr. When a bit-flip error occurrs on one of Q1, Q2 or Q3, this will cause one or both (depending on the error syndrome) of the ancilla pairs to rotate into a singlet state. This allows (subject to complexities discussed in section 2.2.3) tunneling between the electrons in the affected pair, which is registered as a change in dispersive response of the nearby resonator. Thus the error syndrome is immediately detected as a signal in the continuously monitored reflectometry circuit.

2.2.2 Theoretical treatment of scheme with second order perturbation theory

Suppose the system is initally in an arbitrary codespace state, with each of the ancilla pairs starting in triplet states:

$$|\psi(t=0)\rangle = (\alpha\,|\uparrow_{Q1}\downarrow_{Q2}\uparrow_{Q3}\rangle + \beta\,|\downarrow_{Q1}\uparrow_{Q2}\downarrow_{Q3}\rangle)(|\uparrow_{A1}\downarrow_{A3}\rangle + |\downarrow_{A1}\uparrow_{A3}\rangle)(|\uparrow_{A2}\downarrow_{A4}\rangle + |\downarrow_{A2}\uparrow_{A4}\rangle)/2$$

First consider the case where no coupling is applied between the qubits. If we can engineer our system so that $\delta_{1,3}^z = E_{A1}^z - E_{A3}^z \ll 1/T_1$, and similarly $\delta_{2,4}^z \ll 1/T_1$ (with T_1 the timescale of bit flip errors), then the energy difference between the two branches of each qubit singlet is sufficiently small that rate at which the triplets rotate into triplets, and so register a tunnelling event on the reflectometry apparatus, is long compared to the error time and so not limiting. We can see this by considering a single ancilla branch:

$$|\psi(t)\rangle = \frac{1}{\sqrt{2}}(|\uparrow\downarrow\rangle + \exp(-2i\delta t)\,|\downarrow\uparrow\rangle) = \frac{1}{2}\,|T_0\rangle\,(1 + \exp(-2i\delta t)) + \frac{1}{2}\,|S_0\rangle\,(1 - \exp(-2i\delta t))) \tag{2.1}$$

, so that the amplitude of the singlet state goes as

$$|\langle S_0|\psi(t)\rangle|^2 = \sin(\delta t)^2$$

.

Now we apply a coupling between the following four pairs of qubits: Q1 and A1, Q2 and A1, Q2 and A2, Q3 and A2. We consider the four branches of the state in the computational basis of the ancilla qubits seperately, and apply second order perturbation theory to approximate the energy shift of each state due to the adiabatic application of a weak coupling, of strength t. The limits of this approximate treatment will be tested using a numerical simulation developed in chapter 3.

The standard formula for second order perturbation theory is (there is no first-order shift in energy as the perturbing terms are off-diagonal):

$$E_i^1 \approx E_i^0 + \sum_j \frac{|\langle\psi_i|V|\psi_j\rangle|^2}{E_i^0 - E_j^0}$$

where E_i^0 and E_i^1 are the unperturbed and perturbed energies of state i, and H_0 and V are the basic and perturbative hamiltonians. If we set V to the hopping term in the hubbard model, then we obtain, for example,

$$E_{\uparrow\downarrow\uparrow,\uparrow\downarrow,\uparrow\downarrow}^1 - E_{\uparrow\downarrow\uparrow,\uparrow\downarrow,\uparrow\downarrow}^0 = -\frac{t^2}{E_{\uparrow\updownarrow\uparrow,\varnothing\downarrow,\uparrow\downarrow}^0 - E_{\uparrow\downarrow\uparrow,\uparrow\downarrow,\uparrow\downarrow}^0} - \frac{t^2}{E_{\uparrow\varnothing\uparrow,\updownarrow\downarrow,\uparrow\downarrow}^0 - E_{\uparrow\downarrow\uparrow,\uparrow\downarrow,\uparrow\downarrow}^0} - \frac{t^2}{E_{\uparrow\updownarrow\uparrow,\uparrow\downarrow,\varnothing\downarrow}^0 - E_{\uparrow\downarrow\uparrow,\uparrow\downarrow,\uparrow\downarrow}^0} - \frac{t^2}{E_{\uparrow\varnothing\uparrow,\uparrow\downarrow,\updownarrow\downarrow}^0 - E_{\uparrow\downarrow\uparrow,\uparrow\downarrow,\uparrow\downarrow}^0}$$

$$= -t^2\left(\frac{1}{\Delta_1} + \frac{1}{\Delta_2} + \frac{1}{\Delta_3} + \frac{1}{\Delta_4}\right)$$

with

$$\Delta_1 = U_{Q2} + \mu_{Q2} - \mu_{A1} + E_{Q2}^z - E_{A1}^z$$
$$\Delta_2 = U_{A1} + \mu_{A1} - \mu_{Q2} + E_{Q2}^z - E_{A1}^z$$
$$\Delta_3 = U_{Q2} + \mu_{Q2} - \mu_{A2} + E_{Q2}^z - E_{A2}^z$$
$$\Delta_4 = U_{A2} + \mu_{A2} - \mu_{Q2} + E_{Q2}^z - E_{A2}^z$$

Computational branch		Ancilla branch			
Subspace	branch	$\uparrow\downarrow\uparrow\downarrow$	$\uparrow\downarrow\downarrow\downarrow$	$\downarrow\uparrow\uparrow\downarrow$	$\downarrow\uparrow\downarrow\uparrow$
Codespace	$\downarrow\uparrow\downarrow$ / $\uparrow\downarrow\uparrow$	$2\Lambda_t$	$2\Lambda_t$	$2\Lambda_t$	$2\Lambda_t$
E1	$\uparrow\uparrow\downarrow$ / $\downarrow\downarrow\uparrow$	$1\Lambda_t$ / $3\Lambda_t$	$1\Lambda_t$ / $3\Lambda_t$	$3\Lambda_t$ / $1\Lambda_t$	$3\Lambda_t$ / $1\Lambda_t$
E2	$\downarrow\downarrow\downarrow$ / $\uparrow\uparrow\uparrow$	$4\Lambda_t$ / 0	$2\Lambda_t$	$2\Lambda_t$	0 / $4\Lambda_t$
E3	$\downarrow\uparrow\uparrow$ / $\uparrow\downarrow\downarrow$	$1\Lambda_t$ / $3\Lambda_t$	$3\Lambda_t$ / $1\Lambda_t$	$1\Lambda_t$ / $3\Lambda_t$	$3\Lambda_t$ / $1\Lambda_t$

Table 2.1: Table of the (negative) energy shifts due to coupling of each ancilla branch, of each computational branch, of each subspace.

, where the terms describe parameters of the Hubbard model described in section 1.2.1.

We note that $U_i \gg \Delta\mu_i, E_i^z$, and that the magnitude of U_i (order of a few meV) varies little from site to site , so that we may define $\Lambda_t = 2t^2/\langle U_i \rangle$. Then we have

$$E^1_{C\uparrow\downarrow,\uparrow\downarrow} - E^0_{C\uparrow\downarrow,\uparrow\downarrow} = \Delta E_{C\uparrow\downarrow,\uparrow\downarrow} \approx \Delta E_{C\uparrow\downarrow,\downarrow\uparrow} \approx \Delta E_{C\downarrow\uparrow,\uparrow\downarrow} \approx \Delta E_{C\downarrow\uparrow,\downarrow\uparrow} \approx -2\Lambda_t$$

, where we note the shift in energy is the same, within the above approximations, for both of the codespace branches, $|\uparrow\downarrow\uparrow\rangle$ and $|\downarrow\uparrow\downarrow\rangle$, and denote the energies of both branches by the subscript C. All branches of the ancilla state will therefore accure phase at the same rate as long as the state code qubits remains within the codespace.

When a bit-flip error occurs, the state will aquire a component in one of the error subspaces, denoted E1, E2 and E3 depending on which qubit has flipped. Applying the above analysis, we calculate the energy shifts of each of the ancilla branches of each computational branch in each codespace. These are given in table 2.1. These shifts result in the A1, A3, or A2, A4 ancilla pairs rotating from triplets to singlets, or both, depending on the error subspace. To see this, consider the E1 error subspace, into which the state moves when the Q1 qubit experiences a bit-flip error. If both ancilla pairs are in triplet states at the point when the system transitions into the E1 subspace from the codespace, the state undergoes the following evolution [1]:

$$\begin{aligned}
|\psi(t)\rangle =& \alpha\,|\downarrow\downarrow\uparrow\rangle\,(e^{-3i\Lambda_t t}\,|\uparrow\downarrow\uparrow\downarrow\rangle + e^{-3i\Lambda_t t}\,|\uparrow\downarrow\downarrow\downarrow\rangle + e^{-i\Lambda_t t}\,|\downarrow\uparrow\uparrow\downarrow\rangle + e^{-i\Lambda_t t}\,|\downarrow\uparrow\downarrow\uparrow\rangle)/2 \\
&+ e^{-i\delta_{Q1,Q3}t}\beta\,|\uparrow\uparrow\downarrow\rangle\,(e^{-i\Lambda_t t}\,|\uparrow\downarrow\uparrow\downarrow\rangle + e^{-i\Lambda_t t}\,|\uparrow\downarrow\downarrow\downarrow\rangle + e^{-3i\Lambda_t t}\,|\downarrow\uparrow\uparrow\downarrow\rangle + e^{-3i\Lambda_t t}\,|\downarrow\uparrow\downarrow\uparrow\rangle)/2 \\
\approx& \; e^{-3i\Lambda_t t}\alpha\,|\downarrow\downarrow\uparrow\rangle\,(|\uparrow\downarrow\rangle + e^{2i\Lambda_t t}\,|\downarrow\uparrow\rangle)(|\uparrow\downarrow\rangle + |\downarrow\uparrow\rangle)/2 \\
&+ e^{-i\Lambda_t t}\beta\,|\uparrow\uparrow\downarrow\rangle\,(|\uparrow\downarrow\rangle + e^{-2i\Lambda_t t}\,|\downarrow\uparrow\rangle)(|\uparrow\downarrow\rangle + |\downarrow\uparrow\rangle)/2
\end{aligned}$$

, where the $\delta_{Q1,Q3}$ phase term accounts for the difference in energy between the two branches, which is small compared to Λ_t, and irrelevant to our conclusion, so we ignore it. By comparison with equation 2.2.2, we see that the A1,A3 ancilla pair in both branches will rotate into a triplet state with a characteristic timescale $1/\Lambda_t$. The same analysis yields for E2 error subspace:

$$\begin{aligned}
|\psi(t)\rangle \approx& \alpha\,|\downarrow\downarrow\uparrow\rangle\,(|\uparrow\downarrow\rangle + e^{-i\Lambda_t t}\,|\downarrow\uparrow\rangle)(|\uparrow\downarrow\rangle + e^{-i\Lambda_t t}\,|\downarrow\uparrow\rangle)/2 \\
&+ e^{-4i\Lambda_t t}\beta\,|\downarrow\downarrow\uparrow\rangle\,(|\uparrow\downarrow\rangle + e^{i\Lambda_t t}\,|\downarrow\uparrow\rangle)(|\uparrow\downarrow\rangle + e^{i\Lambda_t t}\,|\downarrow\uparrow\rangle)/2
\end{aligned}$$

, so that both pairs of ancillas rotate into singlets (at half the rate vs. the E1 case, but this detail is irrelevant at the timescales discussed). The E3 case is identical to the E1 case with the appropriate qubits exchanged, and leads to only the A2, A4 qubit pair rotating into a singlet.

2.2.3   Further questions related to tunnelling physics

Much work has been done optimising the implementation and and examining the classical physics of reflectometry as a tool for quantum measurement. For a review see, e.g. [3], especially section VIII. During the project the author has not had time to study the physics behind this technique in detail. It appears, however, that present analyses treat the system semi-classically in assuming that an electron tunnels, or does not, within the measurement period

---

[1]We assume that the resultant state is approximately a stationary state of the perturbed hamiltonian.

(i.e. the period of time that the tunneling barrier between the pair of qubits is lowered), and seek to maximise the fidelity with which this charge-shifting event, or lack thereof, is detected. This tunneling event is interpreted as a projective measurement of the singlet/triplet system at the point of measurement, with probabilities of either state given by Born's rule. In the present case this is an insufficient analysis: at any given time, there is necessarily some finite component of the electron pair state that is a singlet, and we need to establish a rate at which tunnelling occurs as a function of the amplitude of this component. A full treatment of this problem probably needs to be formulated in terms of quantum master equations and the theory of quantum decoherence [4].

Time has not permitted me to look into this issue, so at the suggestion of my supervisor I will make the simplifying assumption that any ancilla pair that aquires more than a 10% square-amplitude of singlet immediately tunnels and is hence registered by the dispersive readout device with empirically determined fidelity.

Chapter 3

Methods

3.1 Simulating the hubbard model

This section will discuss the methodology used to perform simulations of scheme described in section 2.2 on a hubbard model of a multiple quantum dot system. The treatment of the error correction scheme described in section 2.2 is necessarily highly approximate due to the complexity of the high-dimensional hilbert space involved (for 7 electrons on 7 sites, the occupation basis is of dimension 3432) and the large number of parameters of the Hubbard model, so makes multiple simplifying assumptions, chiefly the application of second-order perturbation theory and ignoring the site-to-site variance in certain model parameters. It is therefore valuable to simulate the Hubbard model numerically to test the validity of these assumptions in various parameter regimes.

My supervisor Dr. Arvidsson-Shukur have developed a code (yet unpublished), `DotHamiltoniser`, designed to generate Hubbard hamiltonians in an occupation basis given a set of physical parameters (E_i^z, U_i, etc.), as well as to perform low-dimensional time-evolution simulations. This was very helpful at the start of my project to visualise the energy levels of the system and their dependence on coupling, but was not designed for higher dimensional time evolution, and could not be used for this purpose due to performance limitations.

I therefore designed a Hamiltonian simulation code, inspired by the work of Dr Arvidsson-Shuker et al., with the ability to handle higher dimensional systems. The system has three main components:

1. A python extension, `FastHamiltoniser`, written in C, C++ and CUDA, which provides highly performant specialised sparse matrix operations for use in Hamiltonian time evolution;

2. `Hamiltonian`, a python class that builds a Hubbard model Hamiltonian from physical parameters; and

3. `Evolution`, a python class which takes as input a Hamiltonian and a set of continuous time instructions to produce a time evolution of a given starting statevector.

3.1.1 Python extension: `FastHamiltoniser`

Structure of extension

The purpose of the simulator is to solve the Schrödinger equation

$$i\dot{\psi} = H\psi$$

(here expressed in natural units) where ψ is a vector in the occupation basis of a Hubbard Hamiltonian. In order to use Runge-Kutta [**Butcher1996**] methods of integration, we need to be able to calculate this derivative efficiently at an arbitrary time and with arbitrary input. H is typically very sparse, with the only off-diagonal terms given by magnetic drives and hopping couplngs, of which typically only a subset of size linear in the number of qubits are non-zero at a given time.

To perform this calculation efficiently, I implemented the following data structure in C. A `HamiltonianMatrix` object contains basic data about the dimension of the array, as well as an array of pointers to objects of type `Permuter`. Each of these `Permuter` objects stores three arrays of equal length, two of integers representing source and target vector indices, and one of floats representing matrix coefficients, where each entry represents a matrix element. `Permuter`s store a coefficient, which can be changed over time by writing to a single variable, and can be turned on and off. The internal arrays are determined in advance of the simulation by python code, and thereafter only the strength and activations of the `Permuter` objects need be modified during the simulation. For example, one such object provides

all the on-diagonal elements of the matrix, and another might provide all the off-diagonal elements associated with a particular J-coupling between two qubits.

Interaction picture calculation

A further requirement that favoured the development of a custom C backend was the ability to perform simulations in the interaction picture. Performing simulations in the interaction picture is necessary due to the large differences in energy between eigenstates, for example due to the U_i on-site repulsion in some states. With any choice of reference energy in a static basis, there are always states whose phase rotates much faster than the timescale of the evolutions that I wish to simulate, meaning there is no suitable step-size that captures the desired phenomena within reasonable computational time with the simulation remaining stable. Instead, we perform the following transformation to the interaction picture:

$$\dot{\psi}_i = \sum_j H_{ij}\psi_j$$

$$\psi_i \rightarrow \phi_i = e^{-iH_{ii}t}\psi_i$$

$$\Rightarrow \dot{\phi} = \sum_{j \neq i} e^{-i(H_{jj} - H_{ii})t} H_{ij}\phi_j$$

.

Since most off-diagonal terms H_{ij} are zero at most points in time, this results in most states being stationary and lowering the rate of rotation of affected states to a longer timescale that can be simulated. It comes at the cost, however, of introducing a time-dependence into the hamiltonian. I wrote a C function to perform the matrix multiplication, only calculating the phase factors as required.

3.2 Truly continuous error correction prototype

Chapter 4

Discussion

4.1 Conclusions

Bibliography

[1] Takashi Nakajima et al. "Quantum non-demolition measurement of an electron spin qubit". In: *Nature Nanotechnology* 14 (2019). DOI: 10.1038/s41565-019-0426-x. URL: https://doi.org/10.1038/s41565-019-0426-x.

[2] G A Oakes et al. "Fast High-Fidelity Single-Shot Readout of Spins in Silicon Using a Single-Electron Box". In: (2023). DOI: 10.1103/PhysRevX.13.011023.

[3] Florian Vigneau et al. "Probing quantum devices with radio-frequency reflectometry". In: (2023).

[4] Howard M Wiseman. "Quantum trajectories and quantum measurement theory". In: *Quantum and Semiclassical Optics: Journal of the European Optical Society Part B* 8.1 (1996), p. 205.

Appendices

Appendix A

Locked states